NUMERICAL COUPLING STRATEGY FOR EVAPORATING TWO-PHASE FLOW COMPUTATIONS : APPLICATION TO SOLID ROCKET MOTORS

Alaric Sibra, Frédérique Laurent, Angelo Murrone, Joël Dupays, Marc Massot

European Congress on Computational Methods
in Applied Sciences and Engineering (ECCOMAS 2012)
J. Eberhardsteiner et.al. (eds.)
Vienna, Austria, September 10-14, 2012

NUMERICAL COUPLING STRATEGY FOR EVAPORATING TWO-PHASE FLOW COMPUTATIONS : APPLICATION TO SOLID ROCKET MOTORS

A. Sibra[abc], F. Laurent[bc], A. Murrone[a], J. Dupays[a] and M. Massot[bcd]

[a]ONERA - Département d'Energétique Fondamentale et Appliquée (DEFA)
BP80100, 91123 Palaiseau Cedex FRANCE
alaric.sibra@onera.fr, angelo.murrone@onera.fr and joel.dupays@onera.fr

[b] CNRS, UPR 288 - "Laboratoire d'Energétique Moléculaire et Macroscopique, Combustion" (EM2C)
Grande Voie des Vignes, 92295 Chatenay-Malabry, FRANCE
frederique.laurent@ecp.fr and marc.massot@ecp.fr

[c] Ecole Centrale Paris (ECP)
Grande Voie des Vignes, 92295 Chatenay-Malabry, FRANCE

[d] Center for Turbulence Research (CTR)
Stanford University, California 94305-4035, USA
mmassot@stanford.edu

Keywords: Evaporation, Polydisperse two-phase flows, Eulerian Multi-Fluid models, Operator splitting.

Abstract. *In solid rocket motors, aluminum particles are included in the propellant to improve the global performances but the distributed combustion of these droplets is suspected to be a driving mechanism of hydrodynamic instabilities. So the accurate simulation of reactive polydisperse sprays strongly coupled to unsteady gaseous flows appears as a major issue for solid rocket motor optimization. In this paper, we only focus on the evaporation process which is a relevant framework and a first validation step before taking into account combustion aspects. We choose a two size moment Eulerian Multi-Fluid method (MF) which has already proved its efficiency to deal with evaporating polydisperse sprays. The aim of this contribution is threefold : to design a numerical coupling method regarding both physics and requirements of industrial computations, to propose an evaporation scheme dedicated to complex evaporation models for MF systems and to implement both developments in an industrial-oriented code. The proposed time splitting strategy is based on a thorough analysis of the multiple timescale nature of evaporating two-phase flows and the constraint to optimize the cost/accuracy ratio. A series of numerical validations on the evaporation scheme are provided before testing the feasability and the potential of our coupling strategy on a simplified solid rocket motor configuration with the CEDRE code developed at ONERA.*

1 INTRODUCTION

In solid rocket motors, aluminum particles are included in the propellant with a significant mass fraction to improve the global performances by increasing the chamber temperature. The distributed combustion of aluminum droplets in a portion of the chamber and the presence of polydisperse $\mathbf{Al_2O_3}$ residues in the entire volume can have a significant impact on the motor behavior. Mass, momentum and energy exchanges strongly couple the particles and the gaseous phase. As a consequence of this interaction, particles can appreciably modify the flow. Although some remarkable jumps have been done in our understanding of the physics for the past 40 years, the impact of aluminum combustion on the amplification of instability levels is still unclear. So the faithful knowledge of the dispersed phase characteristics such as burning time, heat release and aluminum oxyde residue size are essential to get a reliable prediction of two-phase flow instabilities. Moreover, it has been shown that under certain conditions mass transfer process can be a driving mechanism by amplifying flow disturbances [5]. Nowadays, there is still a lack of numerical simulation tools to predict faithfully two-way interactions between both phases on the motor operation. To improve solid rocket motor design, the accurate simulation of burning polydisperse sprays appears as a key point. In this paper, we limit our study to evaporating polydisperse two-phase flows. Indeed, achieving such a computation is a determining step before performing realistic two-phase flow combustion simulations.

In order to treat polydisperse dilute and moderately dense sprays, we choose a kinetic approach where the spray is described by a number density function (NDF) and its evolution follows the transport Williams-Boltzmann equation. We use the Eulerian Multi-Fluid model [6, 8], which discretizes the NDF through a finite volume approach of the size variable assuming size/velocity and size/temperature correlations in order to reduce the phase space dimension. Systems of conservation equations are then obtained by integration on droplet size intervals. These so called sections are coupled together and to the gas through source terms accounting for the gas-particle and the particle-particle interactions. A major advantage of the Multi-Fluid model is to tackle the polydisperse nature of the liquid phase.

We therefore design a numerical coupling strategy for evaporating sprays based on operator splitting. This time integration method consists in decoupling physical phenomena and treating them in several operators which are integrated separately. This strategy have many advantages but the main one is the possibility to solve each problem such as evaporation with numerical dedicated methods. As a second contribution of this paper, we also introduce a numerical scheme which can deal with complex evaporation models in the context of the Multi-Fluid model (MF). This scheme is used in the splitting strategy which is built on an accurate analysis of the two-way coupling difficulties and considering the requirements of industrial two-phase flow solver.

The paper is organized as follows : section 2 first presents a two size moment Multi-Fluid model adapted for evaporating sprays and its hypotheses. Drag, heating and evaporation models for the droplet-gas coupling are then presented. We analyze the different characteristic times encountered in the physics of evaporating two-phase flows and we establish a time scale hierarchy. In section 3, we highlight the benefit of a time integration strategy based on operator splitting. The numerical requirements deduced from the previous part are used to design a splitting method called the convective RER splitting. Then we present a dedicated evaporation scheme for the MF systems called the SKE scheme. We describe how the new coupling strategy and evaporation scheme are implemented in a 1D research code called SAP1 and in the industrial-oriented ONERA code called CEDRE. Section 4 gives numerical validations of

the new evaporation scheme. Then inert and evaporating two-phase flow computations on a simplified solid rocket motor configuration are proposed in order to show the feasibility of the new coupling strategy for industrial computations. As a reference solution, an inert Lagrangian computation is done to evaluate the potential of the splitting approach before concluding.

2 Modeling unsteady evaporating polydisperse sprays

First, a second order Multi-Fluid model is derived [4]. The aim of such a modeling is to treat the polydisperse phase accurately and to give the right trend for the evolution of the mass distribution of the spray during the evaporation process. The way the set of the Multi-Fluid conservations equations is coupled with the gas equations is detailed. The size discretization as well as two size moment reconstructions provide the ability of the model to handle the droplet size variations. In a second part, different models for the droplet-gas coupling are presented. Finally, a time scale hierarchy is established so that a relevant numerical coupling strategy can be designed.

2.1 A two size moment Multi-Fluid model

At the kinetic level, a dispersed phase of liquid droplets is considered as point particles interacting with a carrier continuous gaseous phase. This polydisperse spray is described by a number density function (NDF) f where the quantity $f(t,\mathbf{x},\mathbf{u},T,S)\mathrm{d}\mathbf{x}\mathrm{d}\mathbf{u}\mathrm{d}T\mathrm{d}S$ denotes the average number of droplets, at a time t, in a volume of size $\mathrm{d}\mathbf{x}$ around a space location $\mathbf{x}$, in a $\mathrm{d}\mathbf{u}\mathrm{d}T\mathrm{d}S$-neighborhood of velocity $\mathbf{u}$, internal temperature T and droplet surface S. A Williams-Boltzmann-type equation is used to describe the evolution of the spray. Neglecting collisions, coalescence and secondary break-up phenomena and focusing on local momentum, mass and heat transfers, the transport equation is:

$$\partial_t f + \mathbf{u}.\partial_{\mathbf{x}} f + \partial_{\mathbf{u}}.(\mathbf{F}f) + \partial_T\left(\frac{\mathbf{H}}{c_{p,l}}f\right) - \partial_S(\mathbf{K}f) = 0 \tag{1}$$

where $\mathbf{F}$ and $\mathbf{H}$ are the drag force and heat transfer per unit mass, $c_{p,l}$ is the pressure specific heat capacity. For moderate velocity and thermal lags, these terms can be modeled by Stokes' laws. In more general cases, corrections depending mainly on the particulate Reynolds number have to be modeled to extend the validity of the exchange terms. For instance, Schiller-Naumann and Ranz-Marschall corrections [11] are often used in combustion chambers. Here, $\mathbf{K}$ is the evaporation rate per unit mass. This term is obtained from evaporation models such as the D^2-law or the infinite liquid-conductivity model. In the following, the continuous gas phase is described with the Euler equations for a perfect fluid and with a perfect gas equation of state but the numerical methods developed here after using a finite volume method are generalizable to the Navier-Stokes equations. As shown in the last part, a 2D solid rocket motor simulation obtained from the CEDRE code will be conducted with the Navier-Stokes formulation.

To follow the evolution of the NDF, two approaches are possible : Lagrangian methods solve accurately the NDF itself through a direct discretization of the transport equation. Nevertheless, the repartition of the mass, momentum and heat source terms at the droplet locations onto the gas Eulerian grid leads to numerical diffusion. Moreover, given the difficulties of Lagrangian approaches to scale up on parallel architectures, the Eulerian approach is an interesting alternative. Eulerian methods are based on moment methods of the NDF giving a set of averaged conservation equations. The first step of the Multi-Fluid model relies on the reduction of the phase space dimension. Considering size/velocity and size/temperature correlations, the phase space

only depends on the droplet size variable. The average velocity and enthalpy are respectively defined as $\bar{\mathbf{u}} = n^{-1}\int \mathbf{u} f \mathrm{d}\mathbf{u}\mathrm{d}T$, $\bar{h} = n^{-1}\int h(T) f \mathrm{d}\mathbf{u}\mathrm{d}T$ where $n = \int f \mathrm{d}\mathbf{u}\mathrm{d}T$ is the droplet number density. Here the enthalpy is directly linked to the temperature such as $\bar{h} = h(T)$. For the other terms, the same formalism is used so that $\forall \phi$, $\bar{\phi} = n^{-1}\int \phi f \mathrm{d}\mathbf{u}\mathrm{d}T$. The closure of the system is obtained through the following assumptions :

[H1] At $(t, \mathbf{x})$ for a given droplet size S, there is only one velocity $\bar{\mathbf{u}}(t, \mathbf{x}, S)$ and the velocity dispersion is zero in each direction.

[H2] At $(t, \mathbf{x})$ for a given droplet size S, there is only one temperature $\bar{T}(t, \mathbf{x}, S)$ and the temperature dispersion is zero.

The following NDF is now only conditionned by droplet size :

$$f(t, \mathbf{x}, \mathbf{u}, T, S) = n(t, \mathbf{x}, S)\delta(\mathbf{u} - \bar{\mathbf{u}}(t, \mathbf{x}, S))\delta(T - \bar{T}(t, \mathbf{x}, S)) \tag{2}$$

This reduces the support of the NDF to a one dimensional sub-manifold parametrized by droplet size. Finally, this step leads to a system of conservation laws called the semi-kinetic model :

$$\left\{ \begin{array}{rl} \partial_t n + \partial_{\mathbf{x}}(n\bar{\mathbf{u}}) & = \partial_S(n\bar{\mathbf{K}}) \\ \partial_t(n\bar{\mathbf{u}}) + \partial_{\mathbf{x}}(n\bar{\mathbf{u}} \otimes \bar{\mathbf{u}}) & = \partial_S(n\bar{\mathbf{K}}\bar{\mathbf{u}}) + n\bar{\mathbf{F}} \\ \partial_t(n\bar{h}) + \partial_{\mathbf{x}}(n\bar{h}\bar{\mathbf{u}}) & = \partial_S(n\bar{\mathbf{K}}\bar{h}) + n\bar{\mathbf{H}} \end{array} \right. \tag{3}$$

The second step to obtain the Eulerian Multi-Fluid model is the finite volume discretization of the size phase space such as $0 = S_1 < ... < S_{\mathrm{N_{sec}}} = \infty$ for the droplet surface variable. An averaged system of conservation equations is obtained for each fixed size interval $[S_{k-1}, S_k[$ called section. The set of droplets in one section can be seen as a "fluid" for which conservation equations are written, the sections exchanging mass, momentum and enthalpy. So as to close the system, three other assumptions are done. The first one is :

[H4] In each section, the form of n can be presumed and expressed as a function of S.

A first way to derive the MF systems is to consider a piecewise constant form for n in each section [8]. In order to study evaporation or coalescence where size changing phenomena occur at any time and location, a two size moment method is more appropriate [4]. Here a piecewise exponential form is chosen for the size distribution, always using the surface variable :

$$n(t, \mathbf{x}, S) = a_k(t, \mathbf{x}) \exp(-b_k(t, \mathbf{x})S), \quad S \in [S_{k-1}, S_k[\tag{4}$$

Since the size distribution function has two parameters, two size moments have to be treated. The size moment of order 0 is the number concentration of droplets and the moment of order $3/2$ matches to the bulk mass density of droplets :

$$n_k(t, \mathbf{x}) = \int_{S_{k-1}}^{S_k} n(t, \mathbf{x}, S)\mathrm{d}S \qquad m_k(t, \mathbf{x}) = \frac{\rho_l}{6\sqrt{\pi}} \int_{S_{k-1}}^{S_k} S^{\frac{3}{2}} n(t, \mathbf{x}, S)\mathrm{d}S \tag{5}$$

where ρ_l is the supposed liquid droplet material density.

Two assumptions are required on the velocity and the temperature to close the MF model :

[H5] In each section, the velocity $\bar{\mathbf{u}}(t, \mathbf{x}, S) = \bar{\mathbf{u}}_{\mathbf{k}}(t, \mathbf{x})$ does not depend on the size of droplets.

[H6] In each section, the temperature $\bar{T}(t, \mathbf{x}, S) = \bar{T}_k(t, \mathbf{x})$ does not depend on the size of droplets.

Finally, the two-phase coupled system of conservation equations based on a two size moment Multi-Fluid model reads :

$$\left\{\begin{array}{rl}
\partial_t \rho_g + \partial_{\mathbf{x}}.(\rho_g \mathbf{u_g}) & = \sum_{k=1}^{\mathrm{N_{sec}}} E_k^{(2)} \\
\partial_t(\rho_g \mathbf{u_g}) + \partial_{\mathbf{x}}.(\rho_g \mathbf{u_g} \otimes \mathbf{u_g}) + \partial_{\mathbf{x}} p & = -\sum_{k=1}^{\mathrm{N_{sec}}} (m_k \bar{\mathbf{F}}_\mathbf{k} - E_k^{(2)} \bar{\mathbf{u}}_\mathbf{k}) \\
\partial_t(\rho_g e_g) + \partial_{\mathbf{x}}.(\rho_g e_g \mathbf{u_g}) + p \partial_{\mathbf{x}}.\mathbf{u_g} & = -\sum_{k=1}^{\mathrm{N_{sec}}} (m_k \bar{\mathbf{H}}_\mathbf{k} - E_k^{(2)} \bar{h}_k) + \sum_{k=1}^{\mathrm{N_{sec}}} m_k \bar{\mathbf{F}}_\mathbf{k} (\mathbf{u_g} - \bar{\mathbf{u}}_\mathbf{k}) \\
\\
\partial_t n_k + \partial_{\mathbf{x}}.(n_k \bar{\mathbf{u}}_\mathbf{k}) & = N_{k+1}(S_k) - N_k(S_{k-1}) \\
\partial_t m_k + \partial_{\mathbf{x}}.(m_k \bar{\mathbf{u}}_\mathbf{k}) & = (E_{k+1}^{(1)} - E_k^{(1)}) - E_k^{(2)} \\
\partial_t(m_k \bar{\mathbf{u}}_\mathbf{k}) + \partial_{\mathbf{x}}.(m_k \bar{\mathbf{u}}_\mathbf{k} \otimes \bar{\mathbf{u}}_\mathbf{k}) & = (E_{k+1}^{(1)} \bar{\mathbf{u}}_{\mathbf{k+1}} - E_k^{(1)} \bar{\mathbf{u}}_\mathbf{k}) - E_k^{(2)} \bar{\mathbf{u}}_\mathbf{k} + m_k \bar{\mathbf{F}}_\mathbf{k} \\
\partial_t(m_k \bar{h}_k) + \partial_{\mathbf{x}}.(m_k \bar{h}_k \bar{\mathbf{u}}_\mathbf{k}) & = (E_{k+1}^{(1)} \bar{h}_{k+1} - E_k^{(1)} \bar{h}_k) - E_k^{(2)} \bar{h}_k + m_k \bar{\mathbf{H}}_\mathbf{k}
\end{array}\right. \quad (6)$$

The Euler gas equations is added to $4\mathrm{N_{sec}}$ equations and consider transport equations for the local density ρ_g, the velocity $\mathbf{u_g}$ and the internal energy $e_g = e^0 + \int c_{v,g} \mathbf{d}T$ with $c_{v,g}$ is the specific volume heat capacity and e^0 is an internal energy calculated at a reference temperature. Since we have restricted the study to moderate dense sprays, the volume fraction of the liquid phase is neglected. The two phases are only coupled by the source terms. Note that for multi-species gases and negligible species diffusion, the mass concentration statement includes also the following species equations when only one species A is evaporating:

$$\left\{\begin{array}{rl}
\partial_t(\rho_g Y_A) + \partial_{\mathbf{x}}.(\rho_g Y_A \mathbf{u_g}) & = \sum_{k=1}^{\mathrm{N_{sec}}} E_k^{(2)} \\
\partial_t(\rho_g Y_k) + \partial_{\mathbf{x}}.(\rho_g Y_k \mathbf{u_g}) & = 0, \quad k \neq A
\end{array}\right. \quad (7)$$

where ρ_g and $\mathbf{u_g}$ are the local density and velocity of the gas mixture.
The source terms $\bar{\mathbf{F}}_\mathbf{k}$, $\bar{\mathbf{H}}_\mathbf{k}$ and $E_k^{(1,2)}$ come from $\mathbf{F}$, $\mathbf{H}$ and $\mathbf{K}$ averaged on a section. Given the size discretization and a reconstruction function, the source terms are :

$$\bar{\mathbf{F}}_\mathbf{k}(t,\mathbf{x}) = \frac{1}{m_k} \frac{\rho_l}{6\sqrt{\pi}} \int_{S_{k-1}}^{S_k} S^{\frac{3}{2}} \bar{\mathbf{F}}(t,x,S,\bar{\mathbf{u}}_\mathbf{k}) n(t,\mathbf{x},S) \mathrm{d}S \quad (8)$$

$$\bar{\mathbf{H}}_\mathbf{k}(t,\mathbf{x}) = \frac{1}{m_k} \frac{\rho_l}{6\sqrt{\pi}} \int_{S_{k-1}}^{S_k} S^{\frac{3}{2}} \bar{\mathbf{H}}(t,x,S,\bar{\mathbf{u}}_\mathbf{k},\bar{T}_k) n(t,\mathbf{x},S) \mathrm{d}S \quad (9)$$

$$E_k^{(2)}(t,\mathbf{x}) = \frac{\rho_l}{6\sqrt{\pi}} \int_{S_{k-1}}^{S_k} S^{\frac{3}{2}} \bar{\mathbf{K}}(t,x,S,\bar{\mathbf{u}}_\mathbf{k},\bar{T}_k) n(t,\mathbf{x},S) \mathrm{d}S \quad (10)$$

$$E_k^{(1)}(t,\mathbf{x}) = \frac{\rho_l}{6\sqrt{\pi}} S_{k-1}^{\frac{3}{2}} \bar{\mathbf{K}}(t,x,S_{k-1},\bar{\mathbf{u}}_\mathbf{k},\bar{T}_k) n(t,\mathbf{x},S_{k-1}) \quad (11)$$

$$N_k(t,\mathbf{x}) = \bar{\mathbf{K}}(t,x,S_{k-1},\bar{\mathbf{u}}_\mathbf{k},\bar{T}_k) n(t,\mathbf{x},S_{k-1}) \quad (12)$$

These terms depend on chosen drag, heat transfer and evaporation models.

2.2 Models for the droplet-gas coupling

In this section, models for the momentum, heat and mass transfers are presented. Although we adapt these models to match the MF formalism, they are only based on physical meanings and do not depend on how the spray or the gas is approached. In the following, we also highlight the characteristic times linked to convective and local coupling phenomena so as to establish a time scale hierarchy and to rationally design the numerical coupling strategy.

2.2.1 Drag and inert droplet heat transfer models

Without loss of generality, we only present Stokes' laws for $\bar{\mathbf{F}}_\mathbf{k}$ and $\bar{\mathbf{H}}_\mathbf{k}$ used in most of the results done in the last part of this contribution. Considering the MF formalism, formulae for the drag force per unit mass and for the heat transfer can be established in each section :

$$\bar{\mathbf{F}}_\mathbf{k} = \frac{\mathbf{u_g} - \bar{\mathbf{u}}_\mathbf{k}}{\bar{\tau}_k^u}, \quad \bar{\mathbf{H}}_\mathbf{k} = c_{p,k}\frac{T_g - \bar{T}_k}{\bar{\tau}_k^T} \tag{13}$$

where $c_{p,k}$ is the liquid heat capacity for the section k. The dynamic and thermal characteristic times $\bar{\tau}_k^u$ and $\bar{\tau}_k^T$ are obtained after derivation of an average diameter on a section k, they are expressed :

$$\bar{\tau}_k^u = \frac{\rho_l(\bar{d}_k^{pq})^2}{18\nu_g}, \quad \bar{\tau}_k^T = \frac{3}{2}\frac{c_{p,k}}{c_{v,g}}Pr\bar{\tau}_k^u \tag{14}$$

where ν_g is the gas dynamic viscosity, Pr is the Prandtl number. The average diameter on a section k with the exponentiel reconstruction is obtained such as :

$$(\sqrt{\pi}\bar{d}_k^{pq})^{(p-q)} = \frac{\int_{S_{k-1}}^{S_k} S^{\frac{p}{2}}\exp(-b_k(t,\mathbf{x})S)\mathrm{d}S}{\int_{S_{k-1}}^{S_k} S^{\frac{q}{2}}\exp(-b_k(t,\mathbf{x})S)\mathrm{d}S} \tag{15}$$

Depending mainly on the particulate Reynolds number, one has to choose the parameters p and q. For instance, $p = 3$ and $q = 1$ are recommanded for the Stokes regime [7]. When studying inert droplets, the average diameter and the characteristic times of each section are constant since the reconstruction function has no time evolution when neglecting coalescence. However, the droplet size distribution of evaporating sprays is no longer constant. So the average diameter and droplet characteristic times are time dependent.

2.2.2 Evaporating and heating models

Note that the kinetic description of the spray cannot be compatible with a temperature profile within the droplet. So the temperature is assumed to be constant within it. Here we propose two evaporation models used for the numerical tests presented in the last part of this contribution.

Evaporating model 1 : Before performing numerical industrial computations with complex evaporation models, we choose a model that offers an interesting framework to easily evaluate evaporation schemes and the coupling strategy. Several assumptions are done :

- Droplet heating regime is neglected. So we consider that droplets have reached and then remained at their saturation temperature T^{sat}.

- Considering no convective correction terms, model 1 is based on the classical D^2-law [13] where the droplet surface S has a linear regression in time :

$$\mathrm{d}_t(S) = -\mathbf{K} \tag{16}$$

Evaporating model 2 : It takes into account droplet heating until the droplet reaches its saturation temperature determined by the local properties of the flow and assuming a local thermodynamic equilibrium. Without loss of generality, the same heat transfer source term as the one used for inert sprays will be used. Once reaching their saturation temperature, droplets vaporize at a rate $\mathbf{K}$ obtained from the thermal Spalding number B_T. So the evaporation process is only controlled by thermal conductivity. We also consider convective correction terms derived from the Nusselt number $\mathbf{Nu_c}$ so that this model is a first step to achieve physical computations. Model 2 also offers a more complex numerical context than model 1 since it is possible to get an evaporation rate $\bar{\mathbf{K}}_\mathbf{k}$ for each section :

$$\bar{\mathbf{K}}_\mathbf{k} = \frac{4\pi\lambda_g}{\rho_l c_{p,g}} \mathbf{Nu_c} \ln(1 + B_{T,k}), \quad B_{T,k} = \frac{c_{p,g}(T_g - \bar{T}_k)}{L_v} \tag{17}$$

where λ_g is the local thermal conductivity of the gas, $c_{p,g}$ is the specific pressure heat capacity of the gas and L_v is the latent heat of vaporization. One has to notice that convective corrections can easily be applied because of the monokinetic hypothesis in each section.

2.3 Numerical difficulties of evaporating polydisperse sprays

Difficulties of modeling two-phase flow physics mainly rely on treating each phenomena as well as properly coupling all of them. Mass, momentum and heat transfers have their own characteristic times which can lead to a very large time scale range problem. Mathematical peculiarities such as stiffness may appear when studying small droplets because of fast relaxation times. For inert two-phase flows with no size variation, this constraint can be easily forecast for the whole duration of the simulation. Now considering droplet evaporation, one has to deal necessarily with small droplets and a dynamical multi-scale problem. The different time scales are presented and then we determine the level of coupling between all fluids supposing a representative time scale hierarchy.

2.3.1 Convective scales

Convective scales of two-phase flows are linked to space and size discretizations. For the gas, the time scale comes from the space discretization. This characteristic time noted τ_g is defined as the time required for the fastest perturbation to cross the smallest length of a mesh cell Δx_{min}:

$$\tau_g = \frac{\Delta x_{min}}{c_0 + |u_g|_{max}} \tag{18}$$

This time is crucial to build the CFL stability and accuracy of most numerical transport schemes. Studying the MF system, there are as many time scales as sections. Indeed, each section has its own velocity $\bar{\mathbf{u}}_\mathbf{k}$. The liquid convection times are defined such as :

$$\bar{\tau_k}^c = \frac{\Delta x_{min}}{|\bar{\mathbf{u}}_\mathbf{k}|_{max}} \tag{19}$$

In subsonic flows, the gas convective time is close to the acoustic characteristic time τ_{acou} which is the time for an acoustic wave to cross the smallest length of a mesh cell. Most of the time, the liquid convection scales are bigger than the gas convective scale. In supersonic flows such as in the nozzle, both gas and liquid convective scales are faster than the acoustic scale. As a strategy benchmark criterion for solid rocket motor simulations, convective scales have to be established in the nozzle.

2.3.2 Local scales

Dynamic and thermal relaxation times As presented in a previous section, the dynamical and thermal relaxation times $\bar{\tau}_k^u$ and $\bar{\tau}_k^T$ depend on the size distribution on each section and they are proportionnal to the square of the average diameter. Consequently, some droplets especially the smallest ones may have faster times scales than time steps used for industrial computations. For instance, an aluminum oxyde droplet with a $100\,\mathrm{nm}$ diameter in a gas flowfield with $\nu_g = 8,55.10^{-5}\,\mathrm{Pa.s}$ has a thermal time response inferior to $10^{-7}\mathrm{s}$. In evaporating two-phase flow simulations, very small droplets will necessarily appear which has to be taken into account to design the numerical coupling strategy. Moreover numerical schemes dedicated to stiff source terms have be chosen. In order to establish a hierarchy between the different time scales, we distinguish droplets on their ability to react to acoustic disturbances :

- Big droplets are those which relax slower the gas varies in a cell : $\min(\bar{\tau_k}^u, \bar{\tau_k}^T) > \tau_g$
- Small droplets are those which relax faster the gas varies in a cell : $\min(\bar{\tau_k}^u, \bar{\tau_k}^T) < \tau_g$

Mass transfer characteristic times Depending on evaporation models, it is possible to estimate the time required for a droplet to completely evaporate. For the D^2-law and droplets of a given diameter d_p , one can get : $\bar{\tau}^m = \pi d_p^2/K$. This characteristic time can be compared to numerical results and gives a relevant mean to highlight the accuracy of a coupling strategy. In this paper, we are more interested in the evaporation time constraint derived from the size discretization of the MF model $\Delta S_k = (S_k - S_{k-1})$. It is the time to evaporate all droplets of a given section : $\bar{\tau}_k^m = \Delta S_k / \bar{\mathbf{K}}_\mathbf{k}$.

2.3.3 Time scale hierarchy and two-way coupling

When considering two-phase flows, there is a two-way coupling between the gas and the dispersed phase which exchange mass, momentum and energy. From a numerical point of view, it can considered as a four-way coupling since the sections are coupled together through mass transfer terms. All interactions are schematically summed up in Figure 1. The problem features $4\mathrm{N}_{\mathrm{sec}}+1$ time scales which caracterize different levels of coupling. For the local scales, we are only interested in $\min(\bar{\tau_k}^m)$ and $\min(\bar{\tau_k}^{(u,T)})$. In the previous paragraph, we show that the mass transfer charateristic times depend strongly on the MF size discretization and does not necessarily lead to fast time scales. Considering the very small droplets that appear in evaporating sprays, the coupling stiffness comes essentially from $\min(\bar{\tau_k}^{(u,T)})$. In most cases, we assume the local time scale hierarchy :

$$\min(\bar{\tau_k}^{(u,T)}) < \min(\bar{\tau_k}^m) \tag{20}$$

For the gas and liquid convection scales, τ_g and $\min(\bar{\tau_k}^c)$ depend on the space discretization. Most of the time in solid rocket motor configurations, the mesh is designed to avoid harsh CFL

requirements especially in the nozzle where the flow is supersonic. Consequently, these are the local time scales which are the source of the stiffness coupling. Finally, the most likely time scale hierarchy for most of our applications is :

$$\min(\bar{\tau_k}^{(u,T)}) < \min(\bar{\tau_k}^{m}) < (\tau_g, \min(\bar{\tau_k}^{c})) \tag{21}$$

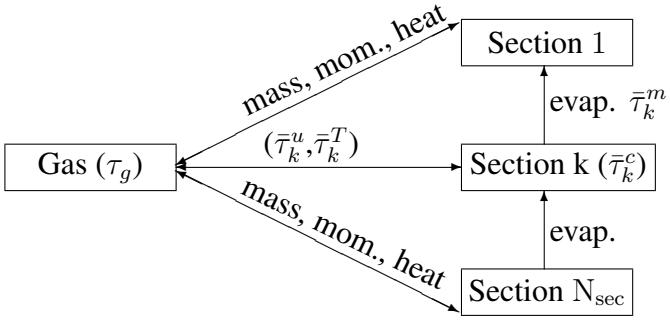

Figure 1: Gas and Multi-Fluid equation coupling and time scales of the system

3 The splitting coupling strategy and numerical methods

In this section, a numerical coupling strategy designed to take into account the main constraints of two-phase flow computations is detailed. On the one hand, difficulties such as the strong coupling between both phases and the stiffness of polydisperse sprays have to be resolved. On the other hand, to be implemented in an industrial-oriented code, the cost/accuracy has to be optimized. The numerical strategy relies on a time operator splitting which decouples gas and liquid convections from the treatment of the coupling source terms. We finally present a new evaporation scheme for the MF models and dedicated to complex evaporation laws.

3.1 The convective RER splitting strategy

3.1.1 Choice of a time splitting integration

One major issue when dealing with strong coupling is the time integration strategy. Two approaches are possible : the first one suggests to integrate simultaneously the gas and liquid system ; one can consider it as a global time strategy. The second one decouples all physical phenomena expressed through several independent operators which are then integrated consecutivetly. This is the principle of splitting techniques. The main problem of an all-at-once integration is to treat properly multiple timescale problems. Plus, it has to be well adapted to solve stiff problems introduced by the fast time scales.

A global explicit time strategy needs a time step smaller than the smallest characteristic time to be stable. Considering evaporating two-phase flows, very small droplets with fast time scales are studied. Another way is to use a global implicit strategy to get stability at higher time steps. Nevertheless, the cross-dependencies between all variables lead to a very complex scheme. Last but not least, having a unique time step and an overall scheme prevent each physical phenomenom to be solved by dedicated numerical schemes with tuned time steps. Plus, one can remember there are several orders of magnitude between the time scales in evaporating two-phase flow simulations.

Here a time splitting technique seems more appropriate to treat multiple time scale problems. The drawbacks of an overall time integration are the advantages of the splitting strategy. The

use of specific numerical methods for each operator and the possibility to have internal time steps respecting their stability conditions enables to gain accuracy on each problem. The main drawback of splitting techniques is a non negligible splitting error when the overall time step is greater than the physical coupling time scales. In the following, we will choose a particular structure of the splitting so as to reduce this error.

3.1.2 Structure of the convective RER splitting

The convective liquid and gas phenomena are decoupled from the coupling processes. Droplet relaxation through the drag force and heat transfer is also solved independently from evaporation. At first sight, it seems not well adapted to separate the heat transfer from the mass transfer. Here the coupling error on the mass transfers strongly depends on the evaporation model since the evaporation rate can be more or less linked to the temperature and velocity variables. In any case, splitting strategies introduce a splitting error but it can minimize if the splitting time step is close to the time scale coupling.

We consider system (7) as composed of transport operators $\mathscr{T}_g$ and $\mathscr{T}_k$'s, a relaxation operator $\mathscr{R}$ and an evaporation one $\mathscr{E}$. These operators apply on $\mathrm{U}(t) \in \mathbb{R}^{4\mathrm{N_{sec}}+3}$, if there is one gas species. Finally, one can write :

$$\mathrm{U}(t) = [\rho_g, \rho_g \mathbf{u_g}, \rho_g e_g, (n_k, m_k, m_k \bar{\mathbf{u}}_\mathbf{k}, m_k \bar{h}_k)_{k=1,\mathrm{N_{sec}}}]^t(t) \tag{22}$$

Note that if there are $\mathrm{N_{spec}}$ gas species, $\mathrm{U}(t) \in \mathbb{R}^{4\mathrm{N_{sec}}+3\mathrm{N_{spec}}+2}$ but in this paper we only present the equations with the gas mixture formalism. The gas transport equation $\mathscr{T}_g$ accounts for full-Mach gaseous dynamics i.e. convection and acoustics :

$$\mathscr{T}_g \left\{ \begin{array}{l} \partial_t \rho_g + \partial_\mathbf{x}.(\rho_g \mathbf{u_g}) = 0 \\ \partial_t (\rho_g \mathbf{u_g}) + \partial_\mathbf{x}.(\rho_g \mathbf{u_g} \otimes \mathbf{u_g}) + \partial_\mathbf{x} p = 0 \\ \partial_t (\rho_g e_g) + \partial_\mathbf{x}.(\rho_g e_g \mathbf{u_g}) + p \partial_\mathbf{x}.\mathbf{u_g} = 0 \end{array} \right. \tag{23}$$

The transport operator for each section k so that the liquid convection occurs independently for all sections :

$$\mathscr{T}_k \left\{ \begin{array}{l} \partial_t n_k + \partial_\mathbf{x}.(n_k \bar{\mathbf{u}}_\mathbf{k}) = 0 \\ \partial_t m_k + \partial_\mathbf{x}.(m_k \bar{\mathbf{u}}_\mathbf{k}) = 0 \\ \partial_t (m_k \bar{\mathbf{u}}_\mathbf{k}) + \partial_\mathbf{x}.(m_k \bar{\mathbf{u}}_\mathbf{k} \otimes \bar{\mathbf{u}}_\mathbf{k}) = 0 \\ \partial_t (m_k \bar{h}_k) + \partial_\mathbf{x}.(m_k \bar{h}_k \bar{\mathbf{u}}_\mathbf{k}) = 0 \end{array} \right. \tag{24}$$

The dynamic and thermal relaxation operator ensures the coupling between the gas and the sections :

$$\mathscr{R} \left\{ \begin{array}{l} \partial_t \rho_g = \partial_t (\rho_g \mathbf{u_g}) = 0 \quad ; \quad \partial_t (\rho_g e_g) = -\sum_{k=1}^{\mathrm{N_{sec}}} m_k \bar{\mathbf{H}}_\mathbf{k} + \sum_{k=1}^{\mathrm{N_{sec}}} m_k \bar{\mathbf{F}}_\mathbf{k} (\mathbf{u_g} - \bar{\mathbf{u}}_\mathbf{k}) \\ \\ \partial_t n_k = \partial_t m_k = 0 \\ \partial_t (m_k \bar{\mathbf{u}}_\mathbf{k}) = m_k \bar{\mathbf{F}}_\mathbf{k} \\ \partial_t (m_k \bar{h}_k) = m_k \bar{\mathbf{H}}_\mathbf{k} \end{array} \right. \tag{25}$$

The evaporation operator treats the mass exchanges between the gas and the sections and be-

tween the sections themselves :

$$\mathscr{E}\begin{cases} \partial_t \rho_g = \sum_{k=1}^{\mathrm{N_{sec}}} E_k^{(2)} \quad ; \quad \partial_t(\rho_g \mathbf{u_g}) = \sum_{k=1}^{\mathrm{N_{sec}}} E_k^{(2)} \bar{\mathbf{u}}_\mathbf{k} \quad ; \quad \partial_t(\rho_g e_g) = \sum_{k=1}^{\mathrm{N_{sec}}} E_k^{(2)} \bar{h}_k \\ \\ \partial_t n_k = N_{k+1}(S_k) - N_k(S_{k-1}) \\ \partial_t m_k = (E_{k+1}^{(1)} - E_k^{(1)}) - E_k^{(2)} \\ \partial_t(m_k \bar{\mathbf{u}}_\mathbf{k}) = (E_{k+1}^{(1)} \bar{\mathbf{u}}_{\mathbf{k+1}} - E_k^{(1)} \bar{\mathbf{u}}_\mathbf{k}) - E_k^{(2)} \bar{\mathbf{u}}_\mathbf{k} \\ \partial_t(m_k \bar{h}_k) = (E_{k+1}^{(1)} \bar{h}_{k+1} - E_k^{(1)} \bar{h}_k) - E_k^{(2)} \bar{h}_k \end{cases} \tag{26}$$

The relaxation and evaporation operators contain the complete coupling of all the "fluids", gas and sections. They both are local in space assuming no convection during the time step. We choose to use a Strang splitting structure [14] to organize all operators. Indeed, until the solution is regular it ensures a second order convergence in time. Moreover, it is known [2] that operators which have the fastest time scales have to be put at the beginning and the end of the splitting. So according to the time scale hierarchy, we suggest the convective RER splitting :

$$\mathrm{U}(t+\Delta t_c) = [\mathscr{R}\mathscr{E}\mathscr{R}]\left(\frac{\Delta t_c}{2}\right) [\sum_{k=1}^{\mathrm{N_{sec}}} \mathscr{T}_k + \mathscr{T}_g](\Delta t_c)\, [\mathscr{R}\mathscr{E}\mathscr{R}]\left(\frac{\Delta t_c}{2}\right) \mathrm{U}(t) \tag{27}$$

and

$$\mathscr{R}\mathscr{E}\mathscr{R}(\Delta t) = \mathscr{R}\left(\frac{\Delta t}{2}\right) \mathscr{E}(\Delta t) \mathscr{R}\left(\frac{\Delta t}{2}\right) \tag{28}$$

In the next part, the evaporation scheme used in operator $\mathscr{E}$ is detailed. This scheme is one of the main contributions of this paper since it is adapted to deal with complex evaporation models in the context of MF systems. Then we present briefly the others schemes for gas and liquid transports and dynamic/thermal relaxation and how they are implemented in two codes dedicated to two-phase flow computations.

3.2 Description of the sectional kinetic evaporation scheme : SKE scheme

Only the evaporation process is studied in this part. Here, we will not integrate directly the mass transfer terms as presented before in eq.(26). A prior study not detailed in this paper shows that explicit methods cannot be stable for reasonable time steps and particular size distributions. An implicit method is possible but still complex and costly. We prefer to choose a kinetic approach adapted to the sectional framework of the MF model. This scheme is called kinetic as it is directly derived from the kinetic equation (1). The size evolution of the droplets follows a transport equation in the size space at the rate $\mathbf{K}$:

$$\partial_t f - \partial_S(\mathbf{K} f) = 0 \tag{29}$$

As done for the derivation of the MF model, a semi-kinetic system is integrated on a section k. Then a system of transport equations at the constant speed $\bar{\mathbf{K}}_\mathbf{k}$ is obtained for $\mathrm{U_k}(t) = [(n_k, m_k, m_k \bar{\mathbf{u}}_\mathbf{k}, m_k \bar{h}_k)_{k=1,\mathrm{N_{sec}}}]^t(t)$:

$$\partial_t \mathrm{U_k} - \bar{\mathbf{K}}_\mathbf{k} \partial_S(\mathrm{U_k}) = 0, \quad k = 1, \mathrm{N_{sec}} \tag{30}$$

The determination of the $\bar{\mathbf{K}}_\mathbf{k}$'s is linked to the choice of the evaporation model. In any case, $\bar{\mathbf{K}}_\mathbf{k} > 0,\ \forall k$. The rates $\bar{\mathbf{K}}_\mathbf{k}$'s can be considered as speeds in the size phase space. To solve the

system, we assume that they are constant during the time step and they are convected at their own velocities. Consequently, at each section boundary, one has to determine the solution of the Riemann problem: when $\bar{\mathbf{K}}_\mathbf{k} > \bar{\mathbf{K}}_{\mathbf{k+1}}$, it is an expansion problem and when $\bar{\mathbf{K}}_\mathbf{k} < \bar{\mathbf{K}}_{\mathbf{k+1}}$, it is a shock problem. Plus, it is possible to have the expression of the shock speed with $n^0 = n(0, S)$ the initial state of the distribution :

$$\bar{\mathbf{K}}_\mathbf{k} < \mathbf{K_m} = \frac{\bar{\mathbf{K}}_{\mathbf{k+1}}\sqrt{n^0(S_k^+)} + \bar{\mathbf{K}}_\mathbf{k}\sqrt{n^0(S_k^-)}}{\sqrt{n^0(S_k^+)} + \sqrt{n^0(S_k^-)}} < \bar{\mathbf{K}}_{\mathbf{k+1}} \tag{31}$$

Now we adopt an explicit resolution of the system with kinetic fluxes and sources. The set of moments $(n_k^{p+1}, m_k^{p+1}, \bar{\mathbf{u}}_\mathbf{k}^{p+1}, \bar{\mathbf{h}}_\mathbf{k}^{p+1})$ at the $p+1$ instant can be derived from the $(n_k^p, m_k^p, \bar{\mathbf{u}}_\mathbf{k}^p, \bar{\mathbf{h}}_\mathbf{k}^p)$ at the p instant assuming that $n(t_{p+1}, S) = n(t_p, S + \bar{\mathbf{K}}_\mathbf{k}\Delta t)$. For the expansion case, the system of moments becomes :

$$\left\{\begin{array}{rcl} n_k^{p+1} & = & \displaystyle\int_{S_{k-1}+\bar{\mathbf{K}}_\mathbf{k}\Delta t}^{S_k+\bar{\mathbf{K}}_{\mathbf{k+1}}\Delta t} n(t_p, S)\mathrm{d}S \\ m_k^{p+1} & = & \displaystyle\int_{S_{k-1}+\bar{\mathbf{K}}_\mathbf{k}\Delta t}^{S_k} (\sigma - \bar{\mathbf{K}}_\mathbf{k}\Delta t)^{\frac{3}{2}} n(t_p, \sigma)\mathrm{d}\sigma + \int_{S_k}^{S_k+\bar{\mathbf{K}}_{\mathbf{k+1}}\Delta t} (\sigma - \bar{\mathbf{K}}_{\mathbf{k+1}}\Delta t)^{\frac{3}{2}} n(t_p, \sigma)\mathrm{d}\sigma \\ m_k^{p+1}\bar{\mathbf{u}}_\mathbf{k}^{p+1} & = & \bar{\mathbf{u}}_\mathbf{k}^p \displaystyle\int_{S_{k-1}+\bar{\mathbf{K}}_\mathbf{k}\Delta t}^{S_k} (\sigma - \bar{\mathbf{K}}_\mathbf{k}\Delta t)^{\frac{3}{2}} n(t_p, \sigma)\mathrm{d}\sigma + \bar{\mathbf{u}}_{\mathbf{k+1}}^p \displaystyle\int_{S_k}^{S_k+\bar{\mathbf{K}}_{\mathbf{k+1}}\Delta t} (\sigma - \bar{\mathbf{K}}_{\mathbf{k+1}}\Delta t)^{\frac{3}{2}} n(t_p, \sigma)\mathrm{d}\sigma \end{array}\right. \tag{32}$$

For the shock case, n_k^{p+1} is the same than before. For a sake of leasibility, only the moment m_k^{p+1} is shown:

$$\left\{\begin{array}{rcl} m_k^{p+1} & = & \displaystyle\int_{S_{k-1}+\bar{\mathbf{K}}_\mathbf{k}\Delta t}^{S_k-\mathbf{K_m}\Delta t+\bar{\mathbf{K}}_\mathbf{k}\Delta t} (\sigma - \bar{\mathbf{K}}_\mathbf{k}\Delta t)^{\frac{3}{2}} n(t_p, \sigma)\mathrm{d}\sigma + \int_{S_{k-1}-\mathbf{K_m}\Delta t+\bar{\mathbf{K}}_{\mathbf{k+1}}\Delta t}^{S_k+\bar{\mathbf{K}}_{\mathbf{k+1}}\Delta t} (\sigma - \bar{\mathbf{K}}_{\mathbf{k+1}}\Delta t)^{\frac{3}{2}} n(t_p, \sigma)\mathrm{d}\sigma \\ & & +(S_k - \bar{\mathbf{K}}_{\mathbf{k+1}}\Delta t)^{\frac{3}{2}} \displaystyle\int_{S_{k-1}-\mathbf{K_m}\Delta t+\bar{\mathbf{K}}_\mathbf{k}\Delta t}^{S_k-\mathbf{K_m}\Delta t+\bar{\mathbf{K}}_{\mathbf{k+1}}\Delta t} n(t_p, \sigma)\mathrm{d}\sigma \end{array}\right. \tag{33}$$

As suggested in section 2.3.2, it is possible to establish a CFL stability criterion for the scheme. First, we define evaporation $\mathrm{CFL_k}$'s on the sections such as :

$$\mathrm{CFL_{k,evap}} = \frac{\Delta t \max(\bar{\mathbf{K}}_\mathbf{k}, \mathbf{K_m})}{(S_k - S_{k-1})} < 1 \tag{34}$$

Finally, we will choose Δt from the most restrictive $\mathrm{CFL_{evap}} = \min(\mathrm{CFL_{evap,k}})$.

3.3 Implementation of the convective RER splitting and dedicated schemes

The convective RER splitting is implemented in two codes : the research code SAP1 (Simulation d'Acoustique Polydisperse 1D) developed at EM2C and the industrial-oriented code CEDRE (Calcul d'Ecoulements Diphasiques Réactifs pour l'Energétique) developed at ONERA. Both can solve a dispersed phase with a two size moment Eulerian MF approach, strongly coupled to a compressible gas. SAP1 code has no cost constraint on the size, space and time

discretizations. High quality numerical methods for structured 1D meshes are implemented but they are not detailed here since no convective aspects are treated with SAP1. Its evaporation scheme is exactly the one described before. The relaxation scheme is based on RADAU5, a fixed error implicit RK5 solver for ODE's with adaptive time step. Note that this scheme is dedicated to stiff problems. The CEDRE code aims at doing research and industrial simulations of complex multi-physics problems. So it is designed to optimize the cost/accuracy ratio. The gas transport schemes is based on second order MUSCL space fluxes. The liquid transport is a first order numerical method inspired from the Bouchut scheme [1] dedicated to pressureless gas dynamics. In a first approach, the dynamic and thermal relaxations are solved explicitly. The evaporation scheme is also the same as the one used in SAP1 but extended to three space dimensions for the momentum equations.

4 Numerical results

This section is structured in two steps which consist first in evaluating the SKE scheme with three different evaporation models. The second is the validation of the convective RER splitting on the simplified motor configuration called TEP considering two computations with inert and then evaporating aluminum droplets in a multispecies gaseous flows. Note that no preliminary 1D validations for the convective/relaxation stage of the splitting is provided since it has already be done in [3] regarding two-phase flow acoustics problems.

4.1 Numerical Tests on the SKE scheme

The following numerical tests are performed on a unique cell mesh since the phenomenon is local in space. Evaporation model 1 is first tested with both SAP1 and CEDRE codes. It is the first validation step because of the constant evaporation for all droplet sizes. This test case was chosen especially to evaluate the behavior of the SKE for low evaporation CFL criterion. The second test uses a smooth evaporation law to check that the scheme is able to deal with different evaporation rates for the sections. Subcases give more specific results on the impact of the size discretization of the MF model. Finally, we assess the SKE scheme on physical problem considering evaporating water droplets exchanging mass and energy with a $\mathbf{H_2O}$ /Air gas mixture at a rate given by evaporation model 2.

4.1.1 Test with evaporation model 1

The simulation starts with an initial number density function; we consider a lognormal distribution L given in eq.(35) over the interval $r \in [\,0\,\mu\mathrm{m}\,;\,45\,\mu\mathrm{m}\,]$ on which we define the indicator function $\mathbb{1}_A$. Such a function is interesting for both mathematical and physical reasons : it is smooth and it corresponds to size distributions that have been observed in solid rockets motors [10]. The size space is discretized with 10 sections and $\Delta S = \mathrm{constant}$.

$$M_{tot} = m_0 \int_0^{+\infty} S^{\frac{3}{2}} L(S) \mathbb{1}_A \mathrm{d}S, \quad L(S) = \frac{1}{S\sigma_{LN}\sqrt{2\pi}} \exp\left(\frac{-(\ln S - \mu_{LN})^2}{2\sigma_{LN}^2}\right) \tag{35}$$

We choose $\sigma_{LN} = 0,3$, $\mu_{LN} = -21,7$ and $M_{tot} = 0.4\,\mathrm{kg/m^3}$; m_0 is a parameter which depends on the liquid mass density. One can write the number of droplets and the bulk mass density in a section k :

$$n_k = m_0 \int_{S_{k-1}}^{S_k} L(S) \mathbb{1}_A \mathrm{d}S \quad ; \quad m_k = m_0 \int_{S_{k-1}}^{S_k} S^{\frac{3}{2}} L(S) \mathbb{1}_A \mathrm{d}S \tag{36}$$

An analytic solution can be established on the NDF : $L(t,S) = L^0(S + \mathbf{K}t)$ which is a translation of the NDF at the constant speed $\mathbf{K}$ in the size space phase. The SKE scheme gives an exact solution when $\mathrm{CFL}_{\mathrm{evap}} = 1$. With $\mathbf{K} = 1.10^{-6}$, the time step is chosen so that the $\mathrm{CFL}_{\mathrm{evap}} \approx 2.10^{-3}$ is low and numerical diffusion in the size phase space may appear. The time

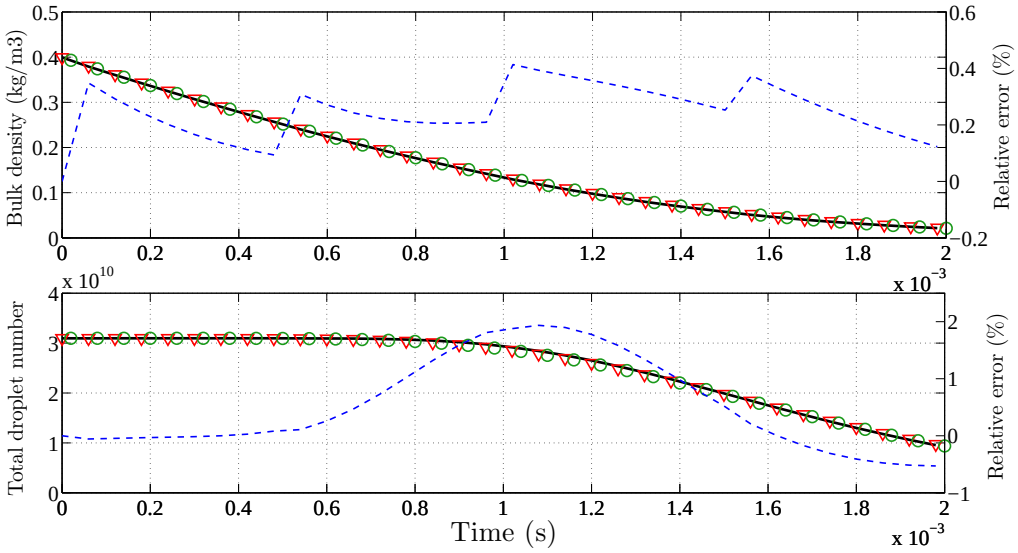

Figure 2: Spray bulk density (top) and total droplet number (bottom) evolutions / CEDRE : ○, SAP1 : ▽, SAP1 error :- -, Analytic solution :**Black**

evolution of the total bulk mass density and the total number of droplets of the spray are good for both SAP1 and CEDRE codes as shown in Figure 2. The relative errors between the analytic solution and SAP1 code are calculated such as :

$$\epsilon_{mass} = \frac{\sum_{k=1}^{\mathrm{N_{sec}}} m_{k,SAP1} - \sum_{k=1}^{\mathrm{N_{sec}}} m_{k,analy.}}{M_{tot}} \qquad \epsilon_{nb} = \frac{\sum_{k=1}^{\mathrm{N_{sec}}} n_{k,SAP1} - \sum_{k=1}^{\mathrm{N_{sec}}} n_{k,analy.}}{N_{tot}} \tag{37}$$

For the bulk mass density, the error does not exceed 0.5%. It is below 2% for the total droplet number. Those errors are quite satisfying because of the chosen low evaporating $\mathrm{CFL}_{\mathrm{evap}}$. Note that the bulk mass density error presents time slots. Their time periods match to the mass transfer characteristic time needed to evaporate completely a section. One may say that these slots illustrates the numerical diffusion of the MF method in the size phase space. Indeed, when considering the exact solution, the sections successively become empty (from the last section to the first one which contains the smallest droplets) but the numerical diffusion tends slightly to keep some droplets in the last sections until their complete evaporation. These slots do not appear in the number error since the number of droplets is relatively low in the last section compared to those in the first ones.

4.1.2 Test with a smooth evaporation law function of S

In this part, we use a larger size range $r \in [\,0\,\mu\mathrm{m}\,;\,60\,\mu\mathrm{m}\,]$. We now consider that $\mathbf{K}$ is no longer constant and depends on the size variable S. This test is appropriate to evaluate the SKE scheme in case of evaporating models like model 2 where the evaporation rate has a

regular evolution in term of droplet size through the regular evolution of the droplet velocity and temperature. This evaporation rate will then be modelized in SKE by a constant by part function of droplet size like the droplet velocity and temperature. An analytic solution resulting from an evaporation law can be obtained assuming a smooth initial NDF. As presented in [9], the solution at time t is:

$$L(t,S) = L^0(\Phi(t;0,S))\frac{\mathbf{K}(\Phi(t;0,S))}{\mathbf{K}(S)} \tag{38}$$

When taking a square root evaporation law $\mathbf{K}(S) = \sqrt{\mathrm{a} + S/S_{max}}$, one can get :

$$\Phi(t;0,S) = S_{max}\left(\left(\frac{t}{2S_{max}} - \sqrt{\mathrm{a} + \frac{S}{S_{max}}}\right) - \mathrm{a}\right) \tag{39}$$

We choose $\mathrm{a} = 1.10^{-10} > 0$ so even the small droplets have a significant evaporation rate. With $S_{max} = 0.2$, the evaporating ratio between the smallest and biggest droplets $\mathbf{K}(\mathrm{N_{sec}})/\mathbf{K}(1) > 10$ is high enough to test harshly the SKE scheme. We first want to assess the scheme not regarding the error due to the size discretization of the MF model. To do this, we take 120 sections. Consequenly, we provide only this test with the research SAP1 code. Note that we get different $\mathrm{CFL_k}$s going from 0.05 to 0.66. With the square root law, the biggest droplets

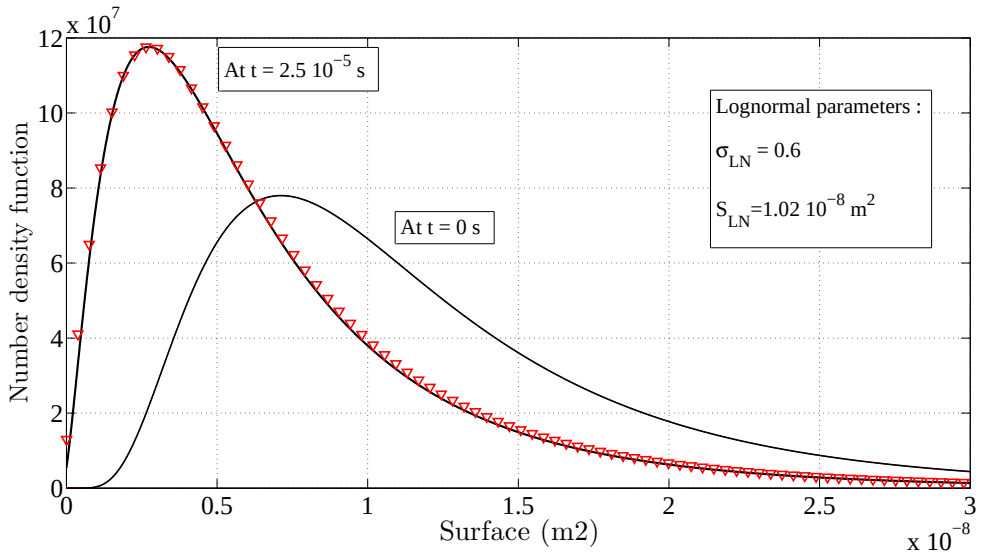

Figure 3: NDF time evolution / SAP1 : ▽, Analytic solution : **Black**

evaporate faster than the smallest ones. We expect that the parameter σ_{LN} of the distribution tend to decrease. As shown in Figure 3, the SKE scheme provides the appropriate time evolution of NDF which tends to prove its ability to deal with smooth evaporation law. At $t = 2.5\,10^{-5}$s, the bulk density error is 0.51% and the error on the total number of droplets is about $2.2\,\%$. These results are quite satisfying and are similar to those obtained with a constant evaporation rate. In industrial computations, few sections are taken for the size discretization in order to minimize the computational cost. So we did the same test case as before but with only 4 sections. The time step is changed and the CFL criterion is 0.24 in the last section. The error on the bulk mass density is about -1% which is very good and a promising result for future industrial applications.

4.1.3 Test with the evaporation model 2 applied on water droplets

We propose to study evaporating water droplets in a two species gas mixture composed of air and water vapor. The simulation starts with a unique size droplet of $d = 20\mu\mathrm{m}$ at a temperature of $293\mathrm{K}$ and a mass fraction of water vapor at 0. The air is initialized at a high temperature of $1500\mathrm{K}$ in order to heat and evaporate completely the 1.10^{-6} mass fraction of the liquid droplets. The size discretization is composed of 10 sections over the interval $r \in [\,0\,\mu\mathrm{m}\,;\,20\,\mu\mathrm{m}\,]$ and $\Delta S = \mathrm{cst}$. To obtain a monodisperse spray i.e. a dirac distribution in the size phase space, the first nine sections are empty and the last section is initialized such as the mass is concentrated on the upper boundary $d_{max} = 20\,\mu\mathrm{m}$. It is an interesting test case in order to evaluate the behavior of the sectional approach with initial discontinuous distributions and also to check the heating and evaporation regimes of model 2. As a reference solution, a Lagrangian approach of the droplets is used. So this simulation was done with CEDRE.

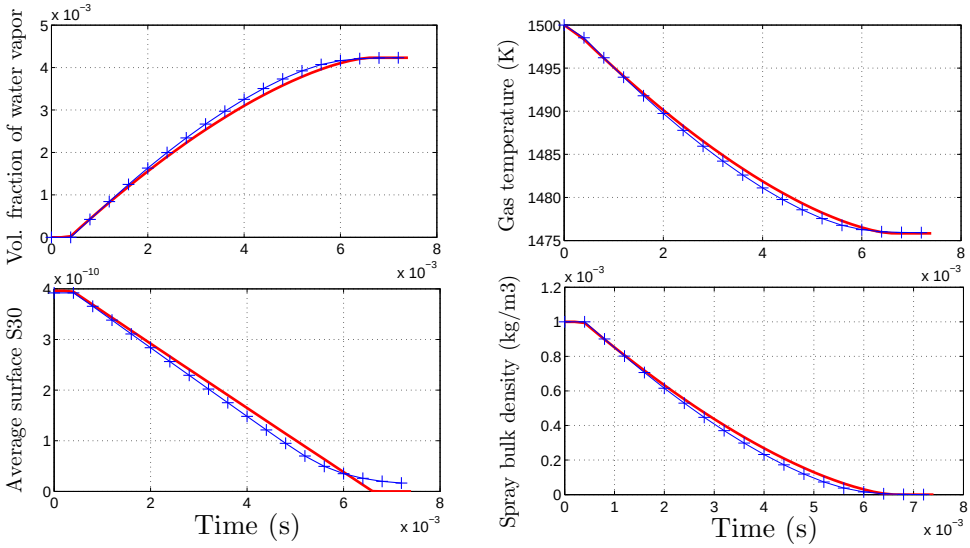

Figure 4: Water droplet and gas variable evolutions / CEDRE Lagrangian : $-$, CEDRE Multi-Fluid : $- + -$

First of all, the time required to heat the droplets about $4.1\,10^{-3}s$, is the same for both approaches. With the MF method, it is possible to get an average surface S_{30} of the whole distribution if considering the same formalism as used in Eq.(15). Note that it is an interesting situation since the gas temperature slightly vary and the evaporation rate is almost constant. So it is similar to consider evaporation model 1 with a time linear regression of the surface. As shown in Figure 4, this behavior is well respected by the SKE scheme. One may notice that the average surface does not equal 0 at the end of the simulation. The explanation is that a very small fraction of the mass remains in the first sections. This bulk mass density portion is about $10^{-8}\,\mathrm{kg/m^3}$ which is very low but sufficient for the code to calculate an average size. The results obtained here are quite good since this test case is really tough. Indeed, the difficulty is to convect a dirac function in the size phase space.

The results of the three test cases validate the SKE scheme. We clearly demonstrate the ability of the SKE scheme to deal with smooth evaporation laws and with low evaporation CFL criterion. The next step is to evaluate this new scheme for multidimensional simulations of evaporation sprays such as in solid rocket motor configurations.

4.2 Inert and evaporating aluminum two-phase flow computations and Lagrangian comparison

The TEP test case is a 2D axisymmetric simplified solid rocket motor configuration. It has been designed as a first approach to validate reactive two-phase flow codes. No hydrodynamic instabilites occur so the motor is studied at steady state. The simulation takes place on a structured 1 470 cell mesh. Both inert and evaporating simulations of this section are initialized with the same pre-established one-phase flow computation. An inert gas species representative of those observed after burning is injected at $3387\,\mathrm{K}$ and at a constant surface flow rate of $10\,\mathrm{kg/m^2/s}$ leading to a normal velocity around $10\,m/s$. The evaporation model used is almost the same as evaporation model 2 i.e. heating and then evaporation but it takes into account convective corrections. In a first part, we choose to test only the relaxation/convective splitting considering inert aluminum droplets. Particles are injected with velocities and temperatures that are different from those of the gas i.e. at the temperature of $2600\,\mathrm{K}$ and a normal velocity of $1\,m/s$. The polydispersity is rendered with a logmormal distribution over the size spectrum $d \in [\,0\,\mu\mathrm{m}\,;\,20\,\mu\mathrm{m}\,]$ and centered on the average diameter $\bar{d}_{30} = 12,37\,\mu\mathrm{m}$. The total droplet surface flow rate is $2\,\mathrm{kg/m^2/s}$ and it is distributed over 4 sections with the injection details given in Tab. 1. The steady stade is reached for a time simulation of $4.10^{-2}\,s$ and the volume fraction repartition in each section is given in Figure 5. With the same injected lognormal distribution, an inert Lagrangian computation is provided. Numerical particles are injected at a period of $1.10^{-6}\,s$. The number of particles in the domain is limited to $400\,000$ but we have an average of more than 50 particles per cell in the constraining nozzle area which is said to be enough to converge on the size and space distribution of the droplets.

	Accessible sizes (μm)	$\bar{d}_{30}$ diameter (μm)	Surface flow rate (kg/m^2/s)
Section 1	$[0.00, 10.00[$	9.39	0.0615
Section 2	$[10.00, 14.14[$	12.21	1.2792
Section 3	$[14.14, 17.32[$	15.22	0.5861
Section 4	$[17.32, 20.00[$	18.14	0.0671

Table 1: Particle injection conditions

First of all, one may check the final pressure at the center of the chamber. For the Lagrangian simulation, we obtain $8.21\,10^5\,\mathrm{Pa}$ whereas the Eulerian approach with the time splitting method gives a pressure of $8.22\,10^5\,\mathrm{Pa}$ which means a relative error about 1.2%. This satisfactory result on pressure is a preliminary step to validate the Eulerian approach since pressure depends on the flow in the nozzle, which is strongly impacted by gas-particle heat transfer, those occuring with fast time scales. We choose to make our result analysis at slice C1 as shown in Figure 5, located at the outlet of the nozzle because this is a zone where both convective and droplet relaxation are harsh to capture. To make the comparison with the Lagrangian simulation, we apply the same procedure as done before in 4.1.3 to get average droplet velocites and temperatures. As shown in Figure 6, the results are satisfying for most of the C1 slice length but not as good near the axis ($\mathrm{Y} = 0\mathrm{m}$). The errors located near the axis come from one of the issues of Eulerian methods which account difficulty for symmetry axis effects. This problem has already been illustrated in [12]. When looking at the spray bulk density, we note an accumulation of droplets near the axis. The velocity and temperature profiles of Figure 6 are quite satisfying and prove that the numerical coupling strategy is a relevant alternative for solid rocket motor computations.

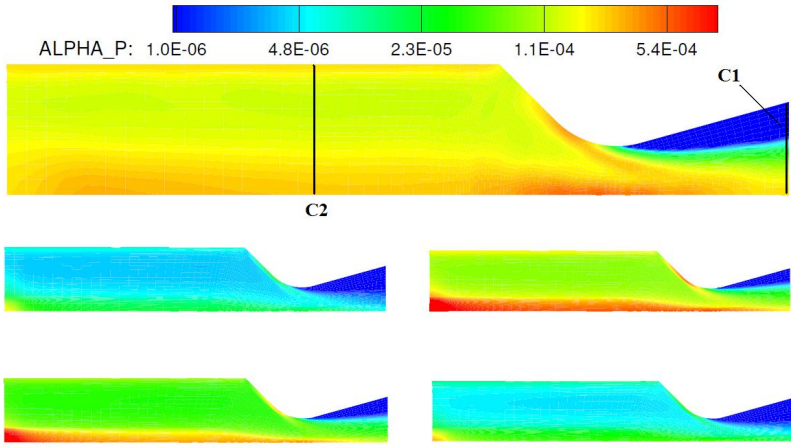

Figure 5: Instantaneous volume fraction : Lagrangian (Top) and Sections (Bottom : Sect. 1 (1,1), Sect. 2 (2,1), Sect. 3 (1,2) and Sect. 4 (2,2)).

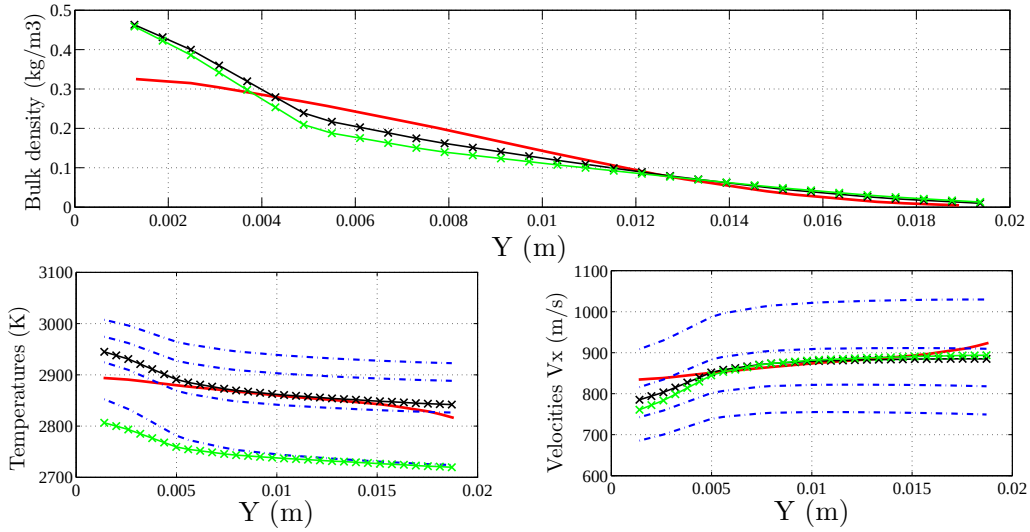

Figure 6: Droplet Bulk density, Vx velocities and temperatures over slice C1 / Lagrangian : $-$, Value of the sections (no evap) : $- \cdot -$ Average MF value no evap. : $-\mathrm{X}-$, Average MF value with evap. : $-\mathrm{X}-$

The validation of the splitting strategy with evaporating aluminum droplets is done by studying the basic features of the evaporating two-phase flows. We first check that the gas temperature at the oulet : it is about $100\,\mathrm{K}$ below the one found in the inert simulation which corresponds to gas energy transferred to latent heat. There is also the right behavior on other variables such as the droplet temperatures. Moreover, we make another slice called C2 as illustrated in Figure 5 along which we plot temperatures and evaporation rates in Figure 7. This gives us information about the heating and the evaporation processes in the chamber. One has to remember that we use an evaporation model which first heat the droplet before evaporating them. In figure 7, we note that there is a heating zone going from the injection surface $\mathrm{Y} = 0.045\,\mathrm{m}$ to a position where the droplets have reached their saturation temperature. Then the droplets evaporate in the rest of the chamber.

All results demonstrate the validity of the SKE in multidimensional configurations and show the feasibility of the convective RER splitting for evaporating two-phase flow computations.

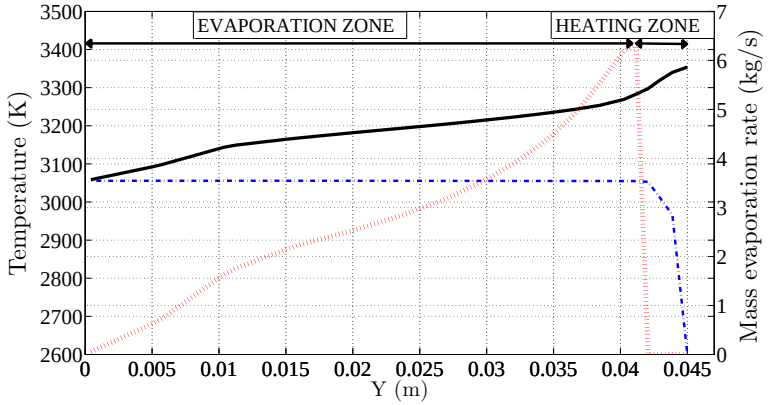

Figure 7: Gas and Section 1 temperatures, Mass evaporation rate over slice C2 / Mass evaporation rate : $\cdots$, Gas : $-$, Droplet : $- \cdot -$

5 CONCLUSIONS

Numerical peculiarities when modeling unsteady evaporating two-phase flows with MF methods have been highlighted. A numerical coupling strategy taking into account the industrial requirements of solid rocket motor computations was proposed. The SKE scheme dedicated to complex evaporation models was developed in the context of MF systems. The scheme was studied and validated on numerical tests involving several evaporation models. Both time splitting strategy and SKE scheme were implemented in the advanced CFD platform CEDRE. As a first step validation for future industrial cases, the results obtained with the simplified TEP configuration confirm that the convective RER splitting is a suitable strategy for droplet-gas coupling with mass exchanges. The time splitting technique also appears as a promising technique for more complex two-phase flow computations accounted for in solid rocket motor physics such as combustion of aluminum polydisperse sprays.

REFERENCES

[1] F. Bouchut, S. Jin, and X. Li. Numerical approximations of pressureless and isothermal gas dynamics. *SIAM J. Num. Anal.*, 41:135–158, 2003.

[2] S. Descombes and M. Massot. Operator splitting for nonlinear reaction-diffusion systems with an entropic structure: singular perturbation and order reduction. *Numer. Math.*, 97(4):667–698, 2004.

[3] F. Doisneau, A. Sibra, J. Dupays, A. Murrone, F. Laurent, and M. Massot. Numerical strategy for two-way coupling in unsteady polydisperse moderately dense sprays. *Submitted to J. Prop. Power*, pages 1–31, 2012. Available on HAL.

[4] G. Dufour and P. Villedieu. A second-order Multi-Fluid model for evaporating sprays. *M2AN Math. Model. Numer. Anal.*, 39(5):931–963, 2005.

[5] J. Dupays. Mass transfer effects on sound propagation in a droplet-gas mixture. In 5^{th} *International Symposium on Special Topics in Chemical Propulsion, Stresa, Italy*, 2000.

[6] J. B. Greenberg, I. Silverman, and Y. Tambour. On the origin of spray sectional conservation equations. *Combustion and Flame*, 93:90–96, 1993.

[7] D. Harrje and F. Reardon. Liquid propellant rocket combustion instability. Technical Report SP - 194, NASA, 1972.

[8] F. Laurent and M. Massot. Multi-fluid modeling of laminar poly-dispersed spray flames: origin, assumptions and comparison of the sectional and sampling methods. *Comb. Theory and Modelling*, 5:537–572, 2001.

[9] M. Massot, F. Laurent, D. Kah, and S. de Chaisemartin. A robust moment method for evaluation of the disappearance rate of evaporating sprays. *SIAM J. Appl. Math.*, 70(8):3203–3234, 2008.

[10] M. Salita. Survey of recent Al_2O_3 droplet size data in Solid Rocket Chambers, Nozzles and Plumes. In 31^{st} *JANNAF Combustion Subcommittee meeting*, Sunnyvale, CA, october 1994.

[11] L. Schiller and A. Naumann. A drag coefficient correlation. *V.D.I Zeitung*, 77:318–320, 1935.

[12] M. Simoes. *Modélisation eulérienne de la phase dispersée dans les moteurs à propergol solide, avec prise en compte de la pression particulaire*. PhD thesis, Institut National Polytechnique de Toulouse, 2006.

[13] D. Spalding. The combustion of liquid fuels. *In Proceedings of the 4th Symp. (Int.) on Combustion, The Comb. Institute*, pages 847–863, 1953. Baltimore.

[14] G. Strang. On the construction and comparison of difference schemes. *SIAM J. Num. Anal.*, 5:507–517, 1968.